Detection of individual gas molecules adsorbed on graphene

F. SCHEDIN[1], A. K. GEIM[1], S. V. MOROZOV[2], E. W. HILL[1], P. BLAKE[1], M. I. KATSNELSON[3] AND K. S. NOVOSELOV[1]*

[1]Manchester Centre for Mesoscience and Nanotechnology, University of Manchester, Manchester, M13 9PL, UK
[2]Institute for Microelectronics Technology, 142432 Chernogolovka, Russia
[3]Institute for Molecules and Materials, University of Nijmegen, 6525 ED Nijmegen, Netherlands
*e-mail: Konstantin.Novoselov@manchester.ac.uk

Published online: 29 July 2007; doi:10.1038/nmat1967

The ultimate aim of any detection method is to achieve such a level of sensitivity that individual quanta of a measured entity can be resolved. In the case of chemical sensors, the quantum is one atom or molecule. Such resolution has so far been beyond the reach of any detection technique, including solid-state gas sensors hailed for their exceptional sensitivity[1–4]. The fundamental reason limiting the resolution of such sensors is fluctuations due to thermal motion of charges and defects[5], which lead to intrinsic noise exceeding the sought-after signal from individual molecules, usually by many orders of magnitude. Here, we show that micrometre-size sensors made from graphene are capable of detecting individual events when a gas molecule attaches to or detaches from graphene's surface. The adsorbed molecules change the local carrier concentration in graphene one by one electron, which leads to step-like changes in resistance. The achieved sensitivity is due to the fact that graphene is an exceptionally low-noise material electronically, which makes it a promising candidate not only for chemical detectors but also for other applications where local probes sensitive to external charge, magnetic field or mechanical strain are required.

Solid-state gas sensors are renowned for their high sensitivity, which—in combination with low production costs and miniature sizes—have made them ubiquitous and widely used in many applications[1,2]. Recently, a new generation of gas sensors has been demonstrated using carbon nanotubes and semiconductor nanowires (see, for example, refs 3,4). The high acclaim received by the latter materials is, to a large extent, due to their exceptional sensitivity allowing detection of toxic gases in concentrations as small as 1 part per billion (p.p.b.). This and even higher levels of sensitivity are sought for industrial, environmental and military monitoring.

The operational principle of graphene devices described below is based on changes in their electrical conductivity, σ, due to gas molecules adsorbed on graphene's surface and acting as donors or acceptors, similar to other solid-state sensors[1–4]. However, the following characteristics of graphene make it possible to increase the sensitivity to its ultimate limit and detect individual dopants. First, graphene is a strictly two-dimensional material and, as such, has its whole volume exposed to surface adsorbates, which maximizes their effect. Second, graphene is highly conductive, exhibiting metallic conductivity and, hence, low Johnson noise even in the limit of no charge carriers[6–9], where a few extra electrons can cause notable relative changes in carrier concentration, n. Third, graphene has few crystal defects[6–10], which ensures a low level of excess $(1/f)$ noise caused by their thermal switching[5]. Fourth, graphene allows four-probe measurements on a single-crystal device with electrical contacts that are ohmic and have low resistance. All of these features contribute to make a unique combination that maximizes the signal-to-noise ratio to a level sufficient for detecting changes in a local concentration by less than one electron charge, e, at room temperature.

The studied graphene devices were prepared by micromechanical cleavage of graphite at the surface of oxidized Si wafers[7]. This allowed us to obtain graphene monocrystals of typically 10 μm in size. By using electron-beam lithography, we made electrical (Au/Ti) contacts to graphene and then defined multiterminal Hall bars by etching graphene in an oxygen plasma. The microfabricated devices (Fig. 1a, upper inset) were placed in a variable temperature insert inside a superconducting magnet and characterized by using field-effect measurements at temperatures, T, from 4 to 400 K and in magnetic fields, B, up to 12 T. This allowed us to find the mobility, μ, of charge carriers (typically, $\approx$5,000 $cm^2\,V^{-1}\,s^{-1}$) and distinguish between single-, bi- and few-layer devices, in addition to complementary measurements of their thickness carried out by optical and atomic force microscopy[6–9]. Figure 1a, lower inset, shows an example of the field-effect behaviour exhibited by our devices at room temperature. This plot shows that longitudinal (ρ_{xx}) and Hall (ρ_{xy}) resistivities are symmetric and antisymmetric functions of gate voltage, V_g, respectively. ρ_{xx} exhibits a peak at zero V_g, whereas ρ_{xy} simultaneously passes through zero, which shows that the transition from electron to hole transport occurs at zero V_g indicating that graphene is in its pristine undoped state[6].

To assess the effect of gaseous chemicals on graphene devices, the insert was evacuated and then connected to a relatively large (5 l) glass volume containing a selected chemical strongly diluted in pure helium or nitrogen at atmospheric pressure. Figure 1b shows the response of zero-field resistivity, $\rho = \rho_{xx}(B = 0) = 1/\sigma$, to NO_2, NH_3, H_2O and CO in concentrations, C, of 1 part per million (p.p.m.). Large easily detectable changes that occurred within 1 min and, for the case of NO_2, practically immediately after letting the chemicals in can be seen. The initial rapid response was followed by a region of saturation, in which the resistivity changed relatively slowly. We attribute this region to redistribution

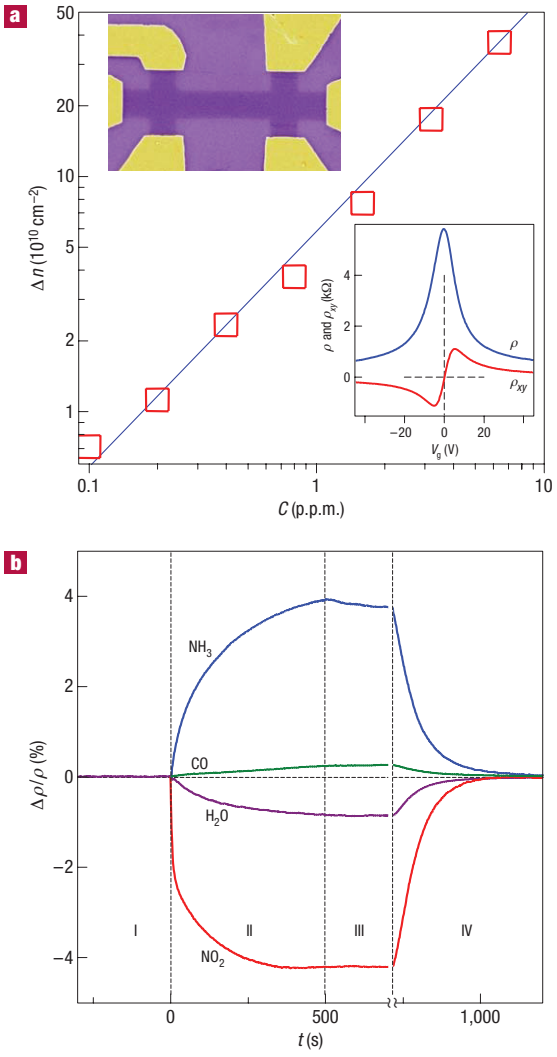

Figure 1 Sensitivity of graphene to chemical doping. a, Concentration, Δn, of chemically induced charge carriers in single-layer graphene exposed to different concentrations, C, of NO_2. Upper inset: Scanning electron micrograph of this device (in false colours matching those seen in visible optics). The scale of the micrograph is given by the width of the Hall bar, which is 1 μm. Lower inset: Characterization of the graphene device by using the electric-field effect. By applying positive (negative) V_g between the Si wafer and graphene, we induced electrons (holes) in graphene in concentrations $n = \alpha V_g$. The coefficient $\alpha \approx 7.2 \times 10^{10}$ cm^{-2} V^{-1} was found from Hall-effect measurements[6–9]. To measure Hall resistivity, ρ_{xy}, $B = 1$ T was applied perpendicular to graphene's surface. **b**, Changes in resistivity, ρ, at zero B caused by graphene's exposure to various gases diluted in concentration to 1 p.p.m. The positive (negative) sign of changes is chosen here to indicate electron (hole) doping. Region I: the device is in vacuum before its exposure; II: exposure to a 5 l volume of a diluted chemical; III: evacuation of the experimental set-up; and IV: annealing at 150 °C. The response time was limited by our gas-handling system and a several-second delay in our lock-in-based measurements. Note that the annealing caused an initial spike-like response in ρ, which lasted for a few minutes and was generally irreproducible. For clarity, this transient region between III and IV is omitted.

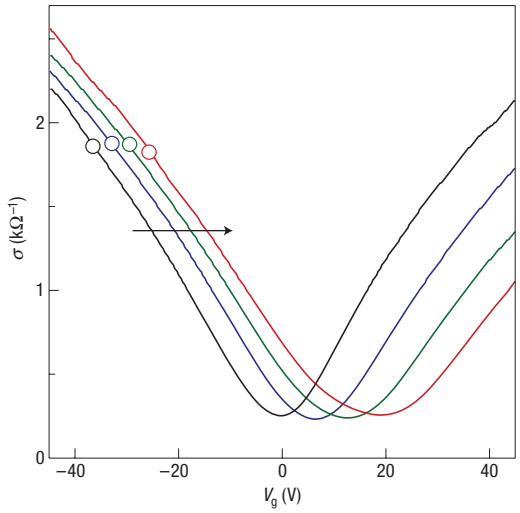

Figure 2 Constant mobility of charge carriers in graphene with increasing chemical doping. Doping increased from zero (black curve) to ~1.5×10^{12} cm^{-2} (red curve) due to increasing exposure to NO_2. Conductivity, σ, of single-layer graphene away from the neutrality point changes approximately linearly with increasing V_g and the steepness of the $\sigma(V_g)$ curves (away from the neutrality point) characterizes the mobility, μ (refs 6–9). Doping with NO_2 adds holes but also induces charged impurities. The latter apparently do not affect the mobility of either electrons or holes. The parallel shift implies a negligible scattering effect of the charged impurities induced by chemical doping. The open symbols on the curves indicate the same total concentration of holes, n_t (~2.7×10^{12} cm^{-2}), as found from Hall measurements. The practically constant σ for the same n_t yields that the absolute mobility, $\mu = \sigma / n_t e$, as well as the Hall mobility are unaffected by chemical doping. For further analysis and discussions, see the Supplementary Information.

of adsorbed gas molecules between different surfaces in the insert. After a near-equilibrium state was reached, we evacuated the container again, which led only to small and slow changes in ρ (region III in Fig. 1b), indicating that adsorbed molecules were strongly attached to the graphene devices at room temperature. Nevertheless, we found that the initial undoped state could be recovered by annealing at 150 °C in vacuum (region IV). Repetitive exposure–annealing cycles showed no 'poisoning' effects of these chemicals (that is, the devices could be annealed back to their initial state). A short-time ultraviolet illumination offered an alternative to thermal annealing.

To gain further information about the observed chemical response, we simultaneously measured changes in ρ_{xx} and ρ_{xy} caused by gas exposure, which allowed us to find directly (1) concentrations, Δn, of chemically induced charge carriers, (2) their sign and (3) mobilities. The Hall measurements revealed that NO_2, H_2O and iodine acted as acceptors, whereas NH_3, CO and ethanol were donors. We also found that, under the same exposure conditions, Δn depended linearly on the concentration, C, of an examined chemical (see Fig. 1a). To achieve the linear conductance response, we electrically biased our devices (by more than ±10 V) to higher-concentration regions, away from the neutrality point, so that both $\sigma = ne\mu$ and Hall conductivity, $\sigma_{xy} = 1/\rho_{xy} = ne/B$, were proportional to n (see Fig. 1a, lower inset)[6–9]. The linear response as a function of C should greatly simplify the use of graphene-based sensors in practical terms.

Chemical doping also induced impurities in graphene in concentrations $N_i = \Delta n$. However, despite these extra scatterers, we found no notable changes in μ even for N_i exceeding 10^{12} cm^{-2}. Figure 2 shows this unexpected observation by showing the electric-field effect in a device repeatedly doped with NO_2. V-shaped $\sigma(V_g)$ curves characteristic for graphene[6–9]

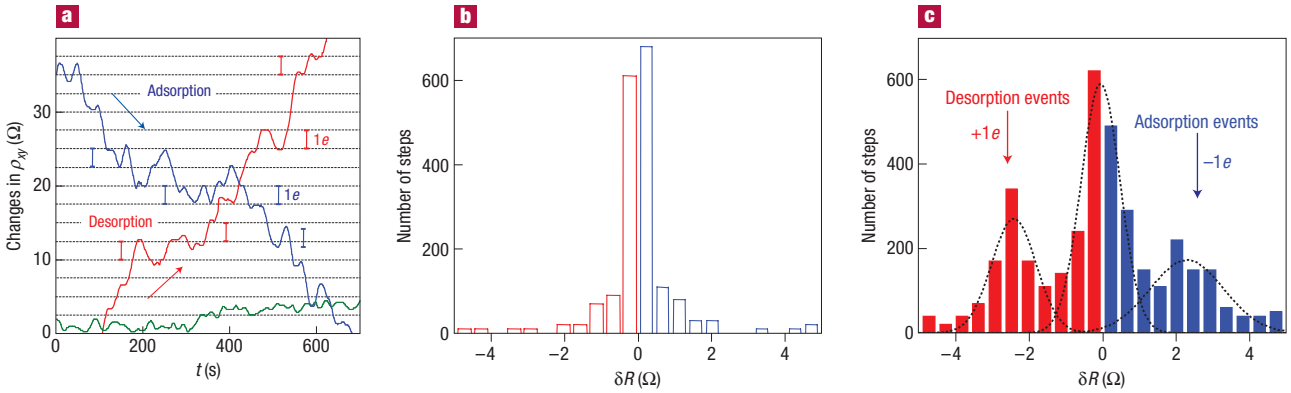

Figure 3 Single-molecule detection. a, Examples of changes in Hall resistivity observed near the neutrality point ($|n| < 10^{11}$ cm^{-2}) during adsorption of strongly diluted NO_2 (blue curve) and its desorption in vacuum at 50 °C (red curve). The green curve is a reference—the same device thoroughly annealed and then exposed to pure He. The curves are for a three-layer device in $B = 10$ T. The grid lines correspond to changes in ρ_{xy} caused by adding one electron charge, e ($\delta R \approx 2.5$ Ω), as calibrated in independent measurements by varying V_g. For the blue curve, the device was exposed to 1 p.p.m. of NO_2 leaking at a rate of $\approx 10^{-3}$ mbar l s^{-1}. **b**,**c**, Statistical distribution of step heights, δR, in this device without its exposure to NO_2 (in helium) (**b**) and during a slow desorption of NO_2 (**c**). For this analysis, all changes in ρ_{xy} larger than 0.5 Ω and quicker than 10 s (lock-in time constant was 1 s making the response time of ≈6 s) were recorded as individual steps. The dotted curves in textbfc are automated gaussian fits (see the Supplementary Information).

can be seen. Their slopes away from the neutrality point provide a measure of impurity scattering (so-called field-effect mobility, $\mu = \Delta\sigma/\Delta ne = \Delta\sigma/e\alpha\Delta V_g$). The chemical doping only shifted the curves as a whole, without any significant changes in their shape, except for the fact that the curves became broader around the neutrality point (the latter effect is discussed in the Supplementary Information). The parallel shift unambiguously proves that the chemical doping did not affect scattering rates. Complementary measurements in magnetic field showed that the Hall-effect mobility, $\mu = \rho_{xy}/\rho_{xx}B$, was also unaffected by the doping and exhibited values very close to those determined from the electric-field effect. Further analysis yields that chemically induced ionized impurities in graphene in concentrations $>10^{12}$ cm^{-2} (that is, less than 10 nm apart) should not be a limiting factor for μ until it reaches values of the order of 10^5 cm^2 V^{-1} s^{-1}, which translates into a mean free path as large as ≈1 μm (see the Supplementary Information). This is in striking contrast with conventional two-dimensional systems, in which such high densities of charged impurities are detrimental for ballistic transport, and also disagrees by a factor of >10 with recent theoretical estimates for the case of graphene[11–13]. Our observations clearly raise doubts about charged impurities being the scatterers that currently limit μ in graphene[11–13]. In the Supplementary Information, we show that a few-nanometre-thick layer of absorbed water provides sufficient dielectric screening to explain the suppressed scattering on charged impurities. We also suggest there that microscopic corrugations of a graphene sheet[14,15] could be dominant scatterers.

The detection limit for solid-state gas sensors is usually defined as the minimal concentration that causes a signal exceeding the sensors' intrinsic noise[1–4]. In this respect, a typical noise level in our devices, $\Delta\rho/\rho \approx 10^{-4}$ (see Fig. 1b), translates into the detection limit of the order of 1 p.p.b. This already puts graphene on par with other materials used for most sensitive gas sensors[1–4]. Furthermore, to demonstrate the fundamental limit for the sensitivity of graphene-based gas sensors, we optimized our devices and measurements as described in the Supplementary Information. In brief, we used high driving currents to suppress the Johnson noise, annealed devices close to the neutrality point, where relative changes in n were largest for the same amount of chemical doping, and used few-layer graphene (typically, 3–5 layers), which allowed a contact resistance of ≈100 Ω, much lower than for single-layer graphene. We also used the Hall geometry that provided the largest response to small changes in n near the neutrality point (see Fig. 1a, lower inset). In addition, this measurement geometry minimizes the sensitive area to the central region of the Hall cross (≈1 μm^2 in size) and allows changes in ρ_{xy} to be calibrated directly in terms of charge transfer by comparing the chemically induced signal with the known response to V_g. The latter is important for the low-concentration region, where the response of ρ_{xy} to changes in n is steepest, but there is no simple relation between ρ_{xy} and n.

Figure 3 shows changes in ρ_{xy} caused by adsorption and desorption of individual gas molecules. In these experiments, we first annealed our devices close to the pristine state and then exposed them to a small leak of strongly diluted NO_2, which was adjusted so that ρ_{xy} remained nearly constant over several minutes (that is, we tuned the system close to thermal equilibrium where the number of adsorption and desorption events within the Hall cross area was reasonably small). In this regime, the chemically induced changes in ρ_{xy} were no longer smooth but occurred in a step-like manner as shown in Fig. 3a (blue curve). If we closed the leak and started to evacuate the sample space, similar steps occurred but predominantly in the opposite direction (red curve). For finer control of the adsorption/desorption rates, we found it useful to slightly adjust the temperature while keeping the same leak rate. The characteristic size, δR, of the observed steps in terms of ohms depended on B, the number of graphene layers and, also, varied strongly from one device to another, reflecting the fact that the steepness of the ρ_{xy} curves near the neutrality point (see Fig. 1a, lower inset) could be different for different devices[6–9]. However, when the steps were recalibrated in terms of equivalent changes in V_g, we found that to achieve the typical value of δR it always required exactly the same voltage changes, ≈1.5 mV, for all of our 1 μm devices and independently of B. The latter value corresponds to $\Delta n \approx 10^8$ cm^{-2} and translates into one electron charge, e, removed from or added to the area of 1×1 μm^2 of the Hall cross (note that changes in ρ_{xy} as a function of V_g were smooth, that is, no charge quantization in the devices' transport characteristics occurred—as expected). As a reference, we repeated

the same measurements for devices annealed for 2 days at 150 °C and found no or very few steps (green curve).

The curves shown in Fig. 3a clearly suggest individual adsorption and desorption events but statistical analysis is required to prove this. To this end, we recorded a large number of curves such as that in Fig. 3a (≈100 h of continuous recording). The resulting histograms with and without exposure to NO_2 are shown in Fig. 3b,c (a histogram for another device is shown in the Supplementary Information). The reference curves exhibited many small (positive and negative) steps, which gave rise to a 'noise peak' at small δR. Large steps were rare. On the contrary, slow adsorption of NO_2 or its subsequent desorption led to many large, single-electron steps. The steps were not equal in size, as expected, because gas molecules could be adsorbed anywhere including the fringes of the sensitive area, which should result in varying contributions. Moreover, because of a finite time constant (1 s) used in these sensitive measurements, random resistance fluctuations could overlap with individual steps either enhancing or reducing them and, also, different events could overlap in time occasionally (such as the largest step on the red curve in Fig. 3a, which has a quadruple height). The corresponding histogram (Fig. 3c) shows the same 'noise peak' as the reference in Fig. 3b but, in addition, there are two extra maxima that are centred at a value of δR, which corresponds to removing/adding one acceptor from the detection area. The asymmetry in the statistical distribution in Fig. 3c corresponds to the fact that single-acceptor steps occur predominantly in one direction, that is, NO_2 on-average desorbs from graphene's surface in this particular experiment. The observed behaviour leaves no doubt that the changes in graphene conductivity during chemical exposure were quantized, with each event signalling adsorption or desorption of a single NO_2 molecule.

In summary, graphene-based gas sensors allow the ultimate sensitivity such that the adsorption of individual gas molecules could be detected. Large arrays of such sensors would increase the catchment area[16], allowing higher sensitivity for short-time exposures and the detection of active (toxic) gases in as minute concentrations as practically desirable. The epitaxial growth of few-layer graphene[17,18] offers a realistic promise of mass production of such devices. Our experiments also show that graphene is sufficiently electronically quiet to be used in single-electron detectors operational at room temperature[19] and in ultrasensitive sensors of magnetic field or mechanical strain[20], in which the resolution is often limited by $1/f$ noise. Equally important[21,22] is the demonstrated possibility of chemical doping of graphene by both electrons and holes in high concentrations without deterioration of its mobility. This should allow microfabrication of p–n junctions, which attract significant interest from the point of view of both fundamental physics and applications. Despite its short history, graphene is considered to be a promising material for electronics by both academic and industrial researchers[6,17,22], and the possibility of its chemical doping further improves the prospects of graphene-based electronics.

Received 14 May 2007; accepted 2 July 2007; published 29 July 2007.

References

1. Moseley, P. T. Solid state gas sensors. *Meas. Sci. Technol.* **8**, 223–237 (1997).
2. Capone, S. *et al.* Solid state gas sensors: State of the art and future activities. *J. Optoelect. Adv. Mater.* **5**, 1335–1348 (2003).
3. Kong, J. *et al.* Nanotube molecular wires as chemical sensors. *Science* **287**, 622–625 (2000).
4. Collins, P. G., Bradley, K., Ishigami, M. & Zettl, A. Extreme oxygen sensitivity of electronic properties of carbon nanotubes. *Science* **287**, 1801–1804 (2000).
5. Dutta, P. & Horn, P. M. Low-frequency fluctuations in solids: 1/f noise. *Rev. Mod. Phys.* **53**, 497–516 (1981).
6. Geim, A. K. & Novoselov, K. S. The rise of graphene. *Nature Mater.* **6**, 183–191 (2007).
7. Novoselov, K. S. *et al.* Two dimensional atomic crystals. *Proc. Natl Acad. Sci. USA* **102**, 10451–10453 (2005).
8. Novoselov, K. S. *et al.* Two dimensional gas of massless Dirac fermions in graphene. *Nature* **438**, 197–200 (2005).
9. Zhang, Y., Tan, J. W., Stormer, H. L. & Kim, P. Experimental observation of the quantum Hall effect and Berry's phase in graphene. *Nature* **438**, 201–204 (2005).
10. Dresselhaus, M. S. & Dresselhaus, G. Intercalation compounds of graphite. *Adv. Phys.* **51**, 1–186 (2002).
11. Ando, T. Screening effect and impurity scattering in monolayer graphene. *J. Phys. Soc. Jpn.* **75**, 074716 (2006).
12. Nomura, K. & MacDonald, A. H. Quantum Hall ferromagnetism in graphene. *Phys. Rev. Lett.* **96**, 256602 (2006).
13. Hwang, E. H., Adam, S. & Das Sarma, S. Carrier transport in two-dimensional graphene layers. *Phys. Rev. Lett.* **98**, 186806 (2007).
14. Morozov, S. V. *et al.* Strong suppression of weak localization in graphene. *Phys. Rev. Lett.* **97**, 016801 (2006).
15. Meyer, J. C. *et al.* The structure of suspended graphene sheets. *Nature* **446**, 60–63 (2007).
16. Sheehan, P. E. & Whitman, L. J. Detection limits for nanoscale biosensors. *Nano Lett.* **5**, 803–807 (2005).
17. Berger, C. *et al.* Electronic confinement and coherence in patterned epitaxial graphene. *Science* **312**, 1191–1196 (2006).
18. Ohta, T., Bostwick, A., Seyller, T., Horn, K. & Rotenberg, E. Controlling the electronic structure of bilayer graphene. *Science* **313**, 951–954 (2006).
19. Barbolina, I. I. *et al.* Submicron sensors of local electric field with single-electron resolution at room temperature. *Appl. Phys. Lett.* **88**, 013901 (2006).
20. Bunch, J. S. *et al.* Electromechanical resonators from graphene sheets. *Science* **315**, 490–493 (2007).
21. Zhou, C., Kong, J., Yenilmez, E. & Dai, H. Modulated chemical doping of individual carbon nanotubes. *Science* **290**, 1552–1555 (2000).
22. Obradovic, B. *et al.* Analysis of graphene nanoribbons as a channel material for field-effect transistors. *Appl. Phys. Lett.* **88**, 142102 (2006).

Acknowledgements

We thank A. MacDonald, S. Das Sarma and V. Falko for illuminating discussions. This work was supported by the EPSRC (UK) and the Royal Society. M.I.K. acknowledges financial support from FOM (Netherlands).
Correspondence and requests for materials should be addressed to K.S.N.
Supplementary Information accompanies this paper on www.nature.com/naturematerials.

Author contributions

K.S.N. designed the experiment and carried out both experimental work and data analysis, A.K.G. suggested the research direction and wrote the manuscript, F.S. and P.B. made graphene devices, S.V.M. and E.W.H. helped with experiments and their analysis and M.I.K. provided theory support. All authors participated in discussions of the research.

Competing financial interests

The authors declare no competing financial interests.